ELSEVIER

Chemical Engineering Journal 138 (2008) 264–273

Chemical Engineering Journal

www.elsevier.com/locate/cej

Effect of high surface area CeO_2 and $Ce\text{-}ZrO_2$ supports over Ni catalyst on CH_4 reforming with H_2O in the presence of O_2, H_2, and CO_2

N. Laosiripojana [a,*], D. Chadwick [b], S. Assabumrungrat [c]

[a] *The Joint Graduate School of Energy and Environment, King Mongkut's University of Technology Thonburi, Bangkok 10140, Thailand*
[b] *Department of Chemical Engineering, Imperial College London SW7 2AZ, UK*
[c] *Center of Excellence on Catalysis and Catalytic Reaction Engineering, Department of Chemical Engineering, Chulalongkorn University, Bangkok 10330, Thailand*

Received 31 January 2007; received in revised form 9 May 2007; accepted 17 May 2007

Abstract

Methane steam reforming over Ni on high surface area (HSA) CeO_2 and $Ce\text{-}ZrO_2$ supports, synthesized by surfactant-assisted method, was studied and compared to conventional Ni/CeO_2, $Ni/Ce\text{-}ZrO_2$, and Ni/Al_2O_3. It was firstly observed that $Ni/Ce\text{-}ZrO_2$ (HSA) with the Ce/Zr ratio of 3/1 showed the best performance in terms of activity and stability. This catalyst presented considerably better resistance toward carbon formation than conventional Ni/CeO_2, $Ni/Ce\text{-}ZrO_2$, and Ni/Al_2O_3; and the minimum inlet H_2O/CH_4 ratio requirement to operate without the detectable of carbon are significantly lower. These benefits are related to the high oxygen storage capacity (OSC) of high surface area $Ce\text{-}ZrO_2$ support. During the reforming process, in addition to the reactions on Ni surface, the redox reactions between the absorbed CH_4 and the lattice oxygen (O_x) on CeO_2 and $Ce\text{-}ZrO_2$ surface also take place, which effectively prevent the formation of carbon on the surface of Ni.

The effects of possible inlet co-reactant, i.e. H_2O, H_2, CO_2, and O_2 on the conversion of CH_4 were also studied. It was found that H_2 presented positive effect on the CH_4 conversion when small amount of H_2 was introduced; nevertheless, this positive effect became less pronounced and eventually inhibited the conversion of CH_4 at high inlet H_2 concentration particularly for Ni/CeO_2 (HSA) and $Ni/Ce\text{-}ZrO_2$ (HSA). The dependence of H_2O on the rate was non-monotonic due to the competition of the active sites, as have also been presented by Xu [1], Xu and Froment [2,3], Elnashaie et al. [4] and Elnashaie and Elshishini [5]. Addition of CO_2 inhibited the reforming rate, whereas addition of O_2 promoted the CH_4 conversion but reduced both CO and H_2 productions.

Keywords: Methane steam reforming; Carbon formation; CeO_2; $Ce\text{-}ZrO_2$

1. Introduction

Methane steam reforming is a widely practiced technology to produce hydrogen or synthesis gas for utilization in chemical processes and solid oxide fuel cells (SOFCs). Three main reactions take place as in the following equations.

$$CH_4 + H_2O = CO + 3H_2 \quad (1)$$

$$CO + H_2O = CO_2 + H_2 \quad (2)$$

$$CH_4 + 2H_2O = CO_2 + 4H_2 \quad (3)$$

Both the water-gas shift reaction (Eq. (2)) and reverse methanation (Eq. (3)) are always associated with catalytic steam reforming at elevated temperatures. Due to their overall high endothermic nature, these reactions are carried out at high-temperature (700–900 °C) to achieve high conversions.

Commercial catalysts for the methane steam reforming reaction are nickel on supports, such as Al_2O_3, MgO, $MgAl_2O_4$ or their mixtures. Selection of a support material is an important issue as it has been evident that metal catalysts are not very active for the steam reforming when supported on inert oxides [6]. Various support materials have been tested, for example, $\alpha\text{-}Al_2O_3$ [7], $\gamma\text{-}Al_2O_3$ and $\gamma\text{-}Al_2O_3$ with alkali metal oxide and rare earth metal oxide [8], $CaAl_2O_4$ [9] and $Ce\text{-}ZrO_2$ [10]. A promising catalyst system for the reforming reactions appears to be a metal on $Ce\text{-}ZrO_2$ support, where the metal can be Ni, Pt or Pd [11–19]. $Ni/Ce\text{-}ZrO_2$ has also been successfully applied to partial oxidation and autothermal reforming of methane [20].

It is well-established that cerium oxide (CeO_2) and ceria-zirconia ($Ce\text{-}ZrO_2$) are useful in a wide variety of applications

* Corresponding author.
E-mail address: navadol_l@jgsee.kmutt.ac.th (N. Laosiripojana).

1385-8947/$ – see front matter © 2007 Elsevier B.V. All rights reserved.
doi:10.1016/j.cej.2007.05.035

involving oxidation or partial oxidation of hydrocarbons (e.g. automotive catalysis) and as components of anodes for SOFCs. This material has high oxygen storage capacity, which is beneficial in oxidation processes and carbon combustion. The excellent resistance toward carbon formation from methane cracking reaction over CeO_2 compared to commercial Ni/Al_2O_3 was also reported recently [21]. The addition of zirconium oxide (ZrO_2) to cerium oxide (CeO_2) has been found to improve the oxygen storage capacity, redox property, thermal stability, and catalytic activity [22–31]. Nevertheless, the major limitations for applying CeO_2 and to a lesser extent $Ce\text{-}ZrO_2$ in high-temperature steam reforming are their low specific surface and surface area reduction due to sintering [21]. Therefore, the use of high surface area (HSA) ceria-based materials as the catalyst support would be a good alternative to improve the methane steam reforming performance. Several methods have been described recently for the preparation of high surface area (HSA) CeO_2 and $Ce\text{-}ZrO_2$ solid solutions. Most interest is focused on the preparation of transition-metal oxides using templating pathways [32–34]. However, only a few of these composites showed a regular pore structure after calcination [35–37]. A surfactant-assisted approach was employed to prepare high surface area CeO_2 and $Ce\text{-}ZrO_2$ with improved textural, structural and chemical properties for environmental applications [38]. They were prepared by reacting a cationic surfactant with a hydrous mixed oxide produced by co-precipitation under basic conditions. By this preparation procedure, materials with good homogeneity and stability especially after thermal treatments were achieved.

In the present work, high surface area (HSA) CeO_2 and $Ce\text{-}ZrO_2$ were synthesized by the surfactant-assisted approach. Ni was selected as a metal catalyst and impregnated on these high surface area CeO_2 and $Ce\text{-}ZrO_2$. It should be noted that, for $Ni/Ce\text{-}ZrO_2$, different ratios of Ce/Zr were firstly investigated to determine a suitable composition ratio. The stability and activity of Ni on high surface area CeO_2 and $Ce\text{-}ZrO_2$ were then studied and compared to Ni on low surface area CeO_2 and $Ce\text{-}ZrO_2$, and also conventional Ni/Al_2O_3. Furthermore, the resistance toward carbon formation and the influences of possible inlet co-reactant, i.e. H_2, H_2O, CO_2, and O_2 (as oxidative steam reforming) on the methane steam reforming over these catalysts were determined by adding and varying the partial pressures of these components at the inlet feed, as these are important issues in the industrial applications.

2. Experimental

2.1. Material preparation and characterization

Conventional $Ce\text{-}ZrO_2$ supports ($Ce\text{-}ZrO_2$ (LSA)) with different Ce/Zr molar ratios were prepared by co-precipitation of cerium chloride ($CeCl_3{\cdot}7H_2O$), and zirconium oxychloride ($ZrOCl_2{\cdot}8H_2O$) from Aldrich. The starting solution was prepared by mixing 0.1 M of metal salt solutions with 0.4 M of ammonia at a 2 to 1 volumetric ratio. This solution was stirred by magnetic stirring (100 rpm) for 3 h, then sealed and placed in a thermostatic bath maintained at 90 °C. The ratio between each metal salt was altered to achieve nominal Ce/Zr molar ratios of 1/3, 1/1 and 3/1. The precipitate was filtered and washed with deionised water and acetone to remove the free surfactant. It was dried overnight in an oven at 110 °C, and then calcined in air at 1000 °C for 6 h.

High surface area (HSA) $Ce\text{-}ZrO_2$ supports were prepared by the surfactant-assisted method [38]. An aqueous solution of an appropriate cationic surfactant and 0.1 M cetyltrimethylammonium bromide solution from Aldrich were added to an 0.1 M aqueous solution containing $CeCl_3{\cdot}7H_2O$ and $ZrOCl_2{\cdot}8H_2O$ in a desired molar ratio. The molar ratio of ([Ce] + [Zr])/[cetyltrimethylammonium bromide] was kept constant at 0.8. The mixture was stirred and then aqueous ammonia was slowly added with vigorous stirring. The mixture was continually stirred for 3 h, then sealed and placed in the thermostatic bath maintained at 90 °C. After that, the mixture was cooled and the resulting precipitate was filtered and washed repeatedly with water and acetone. The filtered powder was dried in the oven at 110 °C for 1 day and then calcined in air at 1000 °C for 6 h. Similarly, CeO_2 (LSA and HSA) were prepared using the same procedures as $Ce\text{-}ZrO_2$, but without the addition of $ZrOCl_2{\cdot}8H_2O$.

$Ni/Ce\text{-}ZrO_2$, Ni/CeO_2 and Ni/Al_2O_3 with 5 wt.% Ni were prepared by impregnating the respective supports with $NiCl_3$ solution at room temperature. These solutions were stirred by magnetic stirring (100 rpm) for 6 h. The solution was dried overnight in the oven at 110 °C, calcined in air at 1000 °C and reduced with 10%H_2 for 6 h. The BET measurements of all synthesized Ni/CeO_2 and $Ni/Ce\text{-}ZrO_2$ were then carried out in order to determine the specific surface area. These values as well as the observed pore volume and pore size of the catalysts are presented in Table 1. It can be seen that the introduction of

Table 1
Specific surface areas, pore volume, and pore size of catalysts after treatments

Catalysts	Surface area after calcination ($m^2\ g^{-1}$)	Pore volume ($cm^3\ g^{-1}$)	Pore size (Å)
$Ni/Ce\text{-}ZrO_2$ (HSA) (Ce/Zr = 1/3)	45	0.15	63.71
$Ni/Ce\text{-}ZrO_2$ (HSA) (Ce/Zr = 1/1)	44	0.14	63.90
$Ni/Ce\text{-}ZrO_2$ (HSA) (Ce/Zr = 3/1)	41.5	0.14	63.15
Ni/CeO_2 (HSA)	24	0.13	63.02
$Ni/Ce\text{-}ZrO_2$ (LSA) (Ce/Zr = 1/3)	20	0.13	63.67
$Ni/Ce\text{-}ZrO_2$ (LSA) (Ce/Zr = 1/1)	18	0.11	61.19
$Ni/Ce\text{-}ZrO_2$ (LSA) (Ce/Zr = 3/1)	19	0.11	62.42
Ni/CeO_2 (LSA)	8.5	0.08	61.20

Table 2
Physicochemical properties of the synthesized catalysts

Catalyst	Metal-load (wt.%)	Metal-reducibility (%)	Ni-dispersion (%)
Ni/Ce-ZrO_2 (HSA) (Ce/Zr = 1/3)	4.9	91.8	9.67
Ni/Ce-ZrO_2 (HSA) (Ce/Zr = 1/1)	4.9	91.0	8.82
Ni/Ce-ZrO_2 (HSA) (Ce/Zr = 3/1)	5.0	92.6	8.95
Ni/CeO_2 (HSA)	5.0	92.2	6.41
Ni/Ce-ZrO_2 (LSA) (Ce/Zr = 1/3)	4.8	90.8	4.69
Ni/Ce-ZrO_2 (LSA) (Ce/Zr = 1/1)	4.9	91.6	4.73
Ni/Ce-ZrO_2 (LSA) (Ce/Zr = 3/1)	4.9	92.1	4.68
Ni/CeO_2 (LSA)	5.0	91.3	3.12
Ni/Al_2O_3	5.0	94.5	4.85

ZrO_2 stabilizes the surface area of catalyst, which is in good agreement with the results obtained on catalysts prepared by conventional routes [21]. It should be noted that the catalysts were also characterized with several physicochemical methods after reduction. The weight content of Ni in Ni/Al_2O_3, Ni/Ce-ZrO_2 (with different Ce/Zr ratio), and Ni/CeO_2 were determined by X-ray fluorescence (XRF) analysis. The reducibility and dispersion percentages of nickel were measured from temperature programmed reduction (TPR) with 5% H_2 in Ar and temperature programmed desorption (TPD), respectively. All physicochemical properties of the synthesized catalysts are presented in Table 2.

2.2. Experimental set-up

Fig. 1 shows the schematic diagram of the experimental reactor system. It consists of three main sections: feed, reaction, and analysis sections. The main obligation of the feed section is to supply the components of interest, such as CH_4, H_2O, H_2, or O_2 to the reaction section, where an 8 mm internal diameter and 40 cm length quartz reactor was mounted vertically inside a furnace. The catalyst (with the weight of 50 mg) was loaded in the quartz reactor, which was packed with a small amount of quartz wool to prevent the catalyst from moving. Preliminary experiments were carried out to find suitable conditions in which internal and external mass transfer effects are not predominant. Considering the effect of external mass transfer, the total flow rate was kept constant at 100 $cm^3\,min^{-1}$ at a constant residence time of 5×10^{-4} g min cm^{-3} in all testing. The suitable average sizes of catalysts were also verified in order to confirm that the experiments were carried out within the region of intrinsic kinetics. In our system, a Type-K thermocouple was placed into the annular space between the reactor and furnace. This thermocouple was mounted in close contact with the catalyst bed to minimize the temperature difference. Another Type-K thermocouple, covering by closed-end quartz tube, was inserted in the middle of the quartz reactor in order to re-check the possible temperature gradient.

After the reactions, the exit gas was transferred via trace-heated lines to the analysis section, which consists of a Porapak Q column Shimadzu 14B gas chromatography (GC) and a mass spectrometer (MS). The gas chromatography was applied in order to investigate the steady state condition experiments, whereas the mass spectrometer was used for the transient carbon formation and water-gas shift reaction experiments.

2.3. Temperature programmed techniques (TP)

In the present work, temperature programmed technique (TP) was applied for studying carbon formation and water-gas shift reaction experiments. Temperature programmed methane adsorption (TPMA) was done in order to investigate the reaction of methane with the surface of catalyst. Five percent CH_4 in He with the total flow rate of 100 $cm^3\,min^{-1}$ was introduced into the system, while the operating temperature increased from room temperature to 900 °C by the rate of 10 °C min^{-1}. Then, the system was cooled down to the room temperature under helium flow. After the TPMA experiment, the carbon deposited on the catalyst was investigated by the temperature programmed oxidation (TPO). Ten percent O_2 in He with the total flow rate of 100 $cm^3\,min^{-1}$ was introduced into the system, after a He purge. Similar to TPMA, the temperature was increased from room temperature to 900 °C. The amount of carbon formation on the surface of each catalyst was then determined by measuring the CO and CO_2 yield obtained from the TPO result.

The temperature programmed reaction (TPR_x) of CO/H_2O/He gas mixture was also carried out in order to investigate the water-gas shift reaction. The mixture of 5%CO and 10%H_2O in He was introduced into the system during heating up period by the rate of 10 °C min^{-1} before reaching the isothermal condition at 900 °C.

3. Results

3.1. Selection of suitable Ce/Zr ratio for Ni/Ce-ZrO_2

Ni/Ce-ZrO_2 catalysts with different Ce/Zr ratios (1/3, 1/1, and 3/1) were firstly tested in methane steam reforming conditions at 900 °C for both HSA and LSA materials in order to select the most suitable ratio of Ce/Zr for the main studies. The results shown in Fig. 2 revealed that at steady state, the Ni/Ce-ZrO_2 with Ce/Zr ratio of 3/1 shows the best performance in terms of stability and activity for both high and low surface areas. Consequently, Ni/Ce-ZrO_2 with Ce/Zr ratio of 3/1 was selected for further investigations.

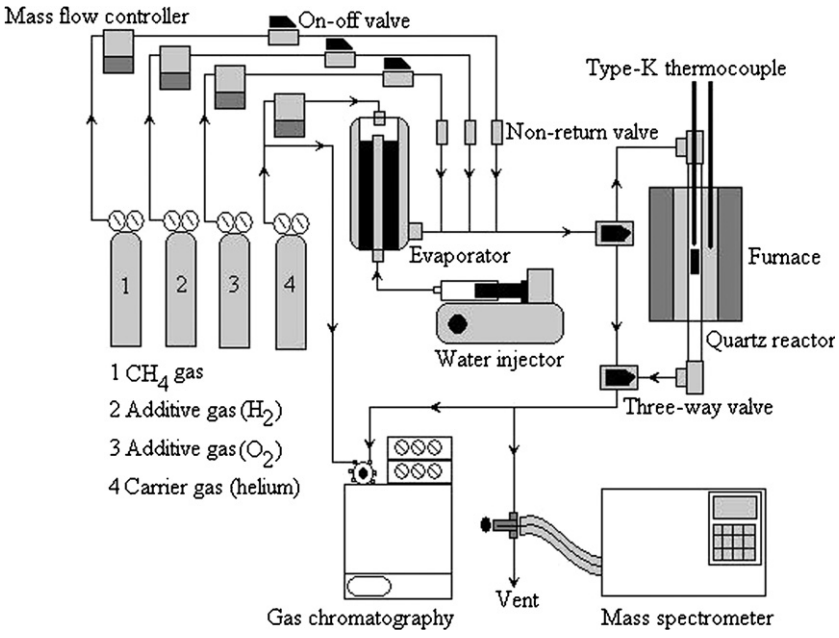

Fig. 1. Schematic diagram of the experimental set-up.

3.2. Stability and activity toward methane steam reforming

The reactivity of methane steam reforming over Ni/CeO_2 (HSA), $Ni/Ce\text{-}ZrO_2$ (HSA) with Ce/Zr ratio of 3/1, Ni/Al_2O_3, $Ni/Ce\text{-}ZrO_2$ (LSA) and Ni/CeO_2 (LSA) were then tested. The inlet components were $CH_4/H_2O/H_2$ in helium with the inlet ratio of 1.0/3.0/0.2 (with the inlet CH_4 partial pressure of 4 kPa). The main products from the reactions over these catalysts were H_2 and CO with some CO_2, indicating a contribution from the water-gas shift, and the reverse methanation at this high-temperature. The steam reforming rate was measured as a function of time in order to indicate the stability and the deactivation rate. The variations in CH_4 conversion with time for different catalysts are shown in Fig. 3. At steady state, Ni/CeO_2 (HSA) and $Ni/Ce\text{-}ZrO_2$ (HSA) presented much higher reactivity toward the methane steam reforming than Ni/Al_2O_3, $Ni/Ce\text{-}ZrO_2$ (LSA), and Ni/CeO_2 (LSA). As seen from the figure, the steam reforming activities of Ni/CeO_2 (LSA) and Ni/Al_2O_3 significantly declined with time before reaching a new steady state rate at a much lower value, while the activity of Ni/CeO_2 (HSA), $Ni/Ce\text{-}ZrO_2$ (HSA), and $Ni/Ce\text{-}ZrO_2$ (LSA) declined slightly. Catalyst stabilities expressed as a deactivation percentage are given in Table 3. In order to investigate the reason of the catalyst deactivation, the post-reaction temperature programmed oxidation (TPO) experiments were then carried out. TPO experiments detected small amount of carbon formation on the surface of Ni over ceria-based supports, whereas significant amount of carbon deposited was observed from the TPO over Ni/Al_2O_3 (1.31 mmol g_{cat}^{-1}). According to these TPO results, the deacti-

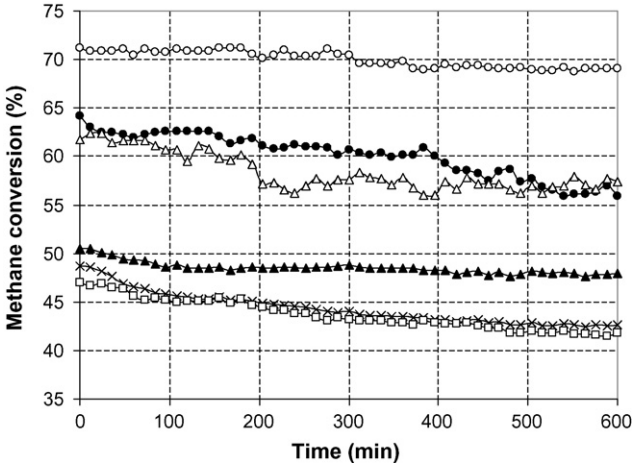

Fig. 2. Steam reforming of methane at 900 °C for $Ni/Ce\text{-}ZrO_2$ with different Ce/Zr ratios using the inlet $CH_4/H_2O/H_2$ ratio of 1.0/3.0/0.2 ($Ni/Ce\text{-}ZrO_2$ (HSA) Ce/Zr = 3/1 (◯), $Ni/Ce\text{-}ZrO_2$ (HSA) Ce/Zr = 1/1 (●), $Ni/Ce\text{-}ZrO_2$ (HSA) Ce/Zr = 1/3 (△), $Ni/Ce\text{-}ZrO_2$ (LSA) Ce/Zr = 3/1 (▲), $Ni/Ce\text{-}ZrO_2$ (LSA) Ce/Zr = 1/1 (×), and $Ni/Ce\text{-}ZrO_2$ (LSA) Ce/Zr = 1/3 (□)).

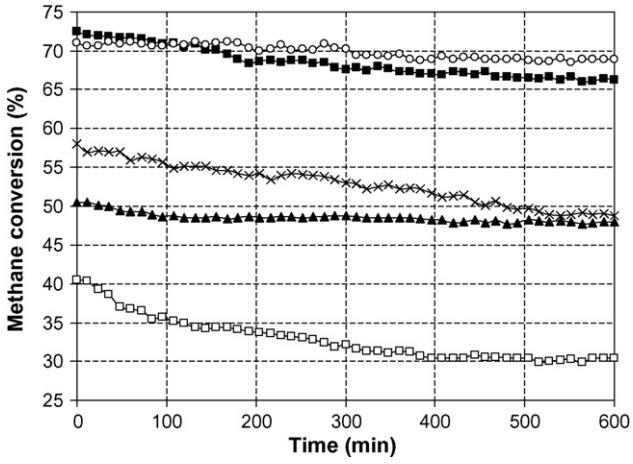

Fig. 3. Steam reforming of methane at 900 °C for different catalysts using the inlet $CH_4/H_2O/H_2$ ratio of 1.0/3.0/0.2 ($Ni/Ce\text{-}ZrO_2$ (HSA) (◯), Ni/CeO_2 (HSA) (■), Ni/Al_2O_3 (×), $Ni/Ce\text{-}ZrO_2$ (LSA) (▲), and Ni/CeO_2 (LSA) (□)).

Table 3
Physicochemical properties of the synthesized catalysts after running the reaction at 900 °C for 10 h

Catalyst	Deactivation (%)	Surface area after reaction ($m^2\ g^{-1}$)	C. formation[a] (mmol g_{cat}^{-1})	Ni-dispersion (%)
Ni/Ce-ZrO_2 (HSA) (Ce/Zr = 1/3)	7.0	42	0.08	9.62
Ni/Ce-ZrO_2 (HSA) (Ce/Zr = 1/1)	12	40	0.11	8.71
Ni/Ce-ZrO_2 (HSA) (Ce/Zr = 3/1)	3.0	40	~0	8.75
Ni/CeO_2 (HSA)	8.7	22	~0	6.33
Ni/Ce-ZrO_2 (LSA) (Ce/Zr = 1/3)	11	18	0.21	4.52
Ni/Ce-ZrO_2 (LSA) (Ce/Zr = 1/1)	12	15	0.19	4.61
Ni/Ce-ZrO_2 (LSA) (Ce/Zr = 3/1)	5.1	18	~0	4.62
Ni/CeO_2 (LSA)	24	6.2	0.14	3.06
Ni/Al_2O_3	16	40	1.31	4.81

[a] Measured from temperature programmed oxidation (TPO).

vation of Ni/Al_2O_3 during the methane steam reforming was mainly related to the carbon formation. In contrast, the deactivations of Ni/CeO_2 and Ni/Ce-ZrO_2 were not caused by the carbon formation; the BET measurement (Table 3) suggested that the deactivations of Ni/CeO_2 and Ni/Ce-ZrO_2, particularly for the low surface area supports, could be due to reduction of surface area. The lower magnitude of the reduction for Ni/CeO_2 (HSA) and Ni/Ce-ZrO_2 (HSA) than for the LSA materials indicates a higher thermal stability for CeO_2 (HSA) and Ce-ZrO_2 (HSA). It should be noted from the BET and TPO studies that although Ni/Al_2O_3 was thermally stable at high operating temperature, it was more susceptible to carbon formation which led to the catalyst deactivation.

3.3. Resistance toward carbon formation

More investigations on the resistance toward the formation of carbon species for all catalysts were investigated by Temperature programmed techniques, i.e. TPMA and TPO. In order to provide the best conditions for testing and obtain the actual resistance toward carbon formation, the influences of exposure time and methane concentration on the amount of carbon formation were firstly determined. Five percent CH_4 in He was fed to the catalyst bed at the isothermal condition (900 °C) for several exposure times (15, 30, 60, 90, 120, 150, and 180 min). The profiles of carbon formation over different catalysts with several exposure times are shown in Fig. 4. Clearly, the quantity of carbon formed on the catalyst surface increased with increasing CH_4 exposure time, and reached its maximum value after 120 min for all catalysts. The influence of inlet CH_4 concentration on the amount of carbon formation was then investigated by introducing different inlet methane partial pressures (2.0–10.0 kPa) with the constant exposure time of 120 min. The amount of carbon deposition seemed to be independent of the inlet methane partial pressure at the same operating conditions. It should be noted that although the rate of carbon formation reaction ($CH_4 \rightarrow C + H_2$) should vary with the methane partial pressure, the reaction time of 120 min may be sufficiently long enough to achieve its maximum carbon formation on the surface of each catalyst and, therefore, the influence of methane partial pressure on coke deactivation was not obviously observed. Therefore, in all experiments, TPMA was carried out by introducing 5% CH_4 in He for 120 min before investigating the degree

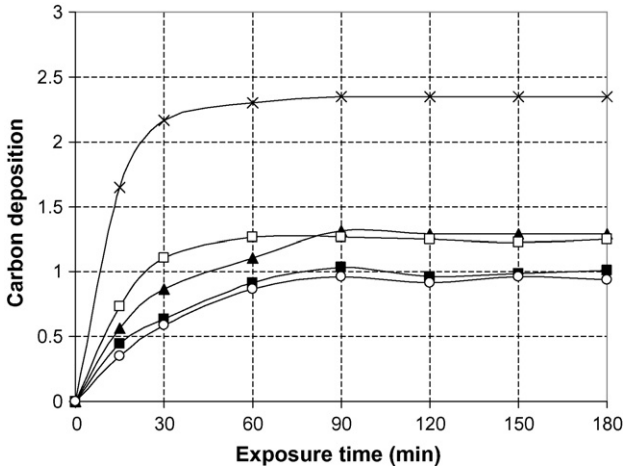

Fig. 4. Influence of exposure time on the amount of carbon formation (mmol g_{cat}^{-1}) for different catalysts at 900 °C (Ni/Ce-ZrO_2 (HSA) (◯), Ni/CeO_2 (HSA) (■), Ni/Al_2O_3 (×), Ni/Ce-ZrO_2 (LSA) (▲), and Ni/CeO_2 (LSA) (□)).

of carbon formation by TPO. Fig. 5 presents the TPMA results for Ni/Ce-ZrO_2 (LSA), Ni/CeO_2 (HSA), Ni/Ce-ZrO_2 (HSA), and Ni/Al_2O_3, while Fig. 6 presents the TPO results for those catalysts.

As seen in Fig. 5, carbon monoxide and carbon dioxide were also produced together with hydrogen for Ni catalysts on ceria-

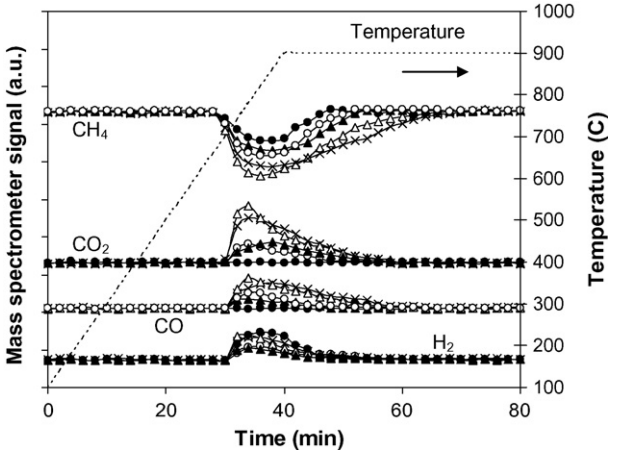

Fig. 5. TPMA over (△) Ni/CeO_2-ZrO_2 (HSA), (×) Ni/CeO_2 (HSA), (◯) Ni/CeO_2-ZrO_2 (LSA), (▲) Ni/CeO_2 (LSA), and (●) Ni/Al_2O_3.

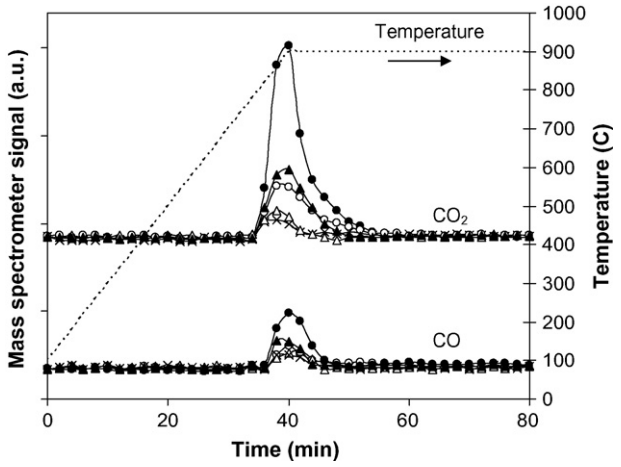

Fig. 6. Temperature programmed oxidation over (△) Ni/CeO_2-ZrO_2 (HSA), (×) Ni/CeO_2 (HSA), (◯) Ni/CeO_2-ZrO_2 (LSA), (▲) Ni/CeO_2 (LSA), and (●) Ni/Al_2O_3 following TPMA to 900 °C.

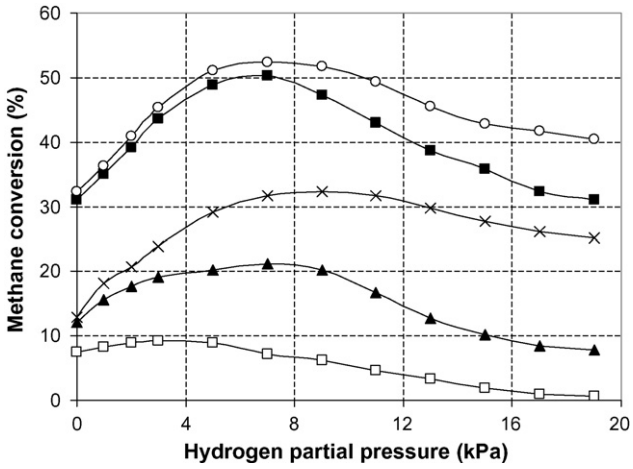

Fig. 7. Effect of hydrogen partial pressure on steam reforming rate over different catalysts at 800 °C (Ni/Ce-ZrO_2 (HSA) (◯), Ni/CeO_2 (HSA) (■), Ni/Al_2O_3 (×), Ni/Ce-ZrO_2 (LSA) (▲), and Ni/CeO_2 (LSA) (□)).

based supports, whereas only hydrogen peak was detected for TPMA over Ni/Al_2O_3. The CO and CO_2 formations from TPMA of Ni catalysts on ceria-based supports comes from the gas–solid reaction of CH_4 with the lattice oxygen (O_x) on ceria surface (Eq. (4)):

$$CH_4 + O_x = 2H_2 + CO + V_O^{\bullet\bullet} + 2e' \quad (4)$$

$V_O^{\bullet\bullet}$ denotes an oxygen vacancy with an effective charge 2^+, e' is an electron which can either be more or less localized on a cerium ion or delocalized in a conduction band. The quantities of carbon deposited (mmol g_{cat}^{-1}) on the surface of each catalyst, which could be calculated by measuring the CO and CO_2 yields, are presented in Table 4. Clearly, Ni/CeO_2 (HSA) and Ni/Ce-ZrO_2 (HSA) provided higher resistance toward carbon formation than Ni/Al_2O_3, Ni/Ce-ZrO_2 (LSA), and Ni/CeO_2 (LSA).

The influence of adding H_2O along with CH_4 at the feed on the amount of carbon formation was studied by varying the inlet H_2O/CH_4 ratio from 0.0/0.05 to 0.15/0.05. As seen in Table 4, it was observed that the carbon deposition over nickel catalyst on ceria-based supports rapidly decreased with increasing inlet steam partial pressure. Nickel catalyst on low surface area (LSA) Ce-ZrO_2 required inlet H_2O/CH_4 ratio of 3.0 in order to prevent the formation of carbon species on catalyst surface, while nickel catalyst on high surface area (HSA) Ce-ZrO_2 required inlet H_2O/CH_4 ratio as low as 1.0. It should be noted that Ni/Al_2O_3 required much higher H_2O/CH_4 ratio to reduce the carbon formation, and the carbon species remains detectable on the surface of Ni/Al_2O_3 even the inlet H_2O/CH_4 ratio is higher than 3.0.

3.4. Effect of inlet co-reactant compositions

The influences of possible co-reactant compositions, i.e. H_2, H_2O, CO_2, and O_2 on the conversion of CH_4 over these Ni catalysts were investigated. First, various inlet H_2 partial pressures were added along with CH_4 and H_2O to the feed in order to investigate the influence of this component on the CH_4 conversion. The inlet CH_4 and H_2O partial pressures were kept constant at 4.0 and 12.0 kPa, respectively. As shown in Fig. 7, with the presence of low H_2 partial pressure (0–5 kPa), H_2 presented positive effect on the CH_4 conversion. Without inlet hydrogen, the CH_4 conversions for all catalysts were apparently low, suggesting that some hydrogen must be fed together with methane and steam to obtain significant reforming rate. Similar result was earlier reported over Ni/ZrO_2 [1]. Table 5 gives the reaction orders in H_2 for all catalysts in this range of H_2 partial pressure. Compared to Ni/Al_2O_3, the reaction orders in hydrogen for Ni catalyst on ceria-based supports, especially on high surface area (HSA) supports were significantly lower. The CH_4 conversion at higher inlet H_2 partial pressures (>5 kPa) was also measured. When the inlet hydrogen partial pressure was greater than 8–10 kPa, a strong reduction in rate was observed for all catalysts, Fig. 7, as expected.

Fig. 8 shows the effect of steam on the CH_4 conversion. It was found that the conversion increased with increasing inlet H_2O partial pressure at low values but H_2O then presented a negative effect on the reforming rate at higher inlet H_2O/CH_4 ratio. It should be noted that the steam requirement for Ni/CeO_2

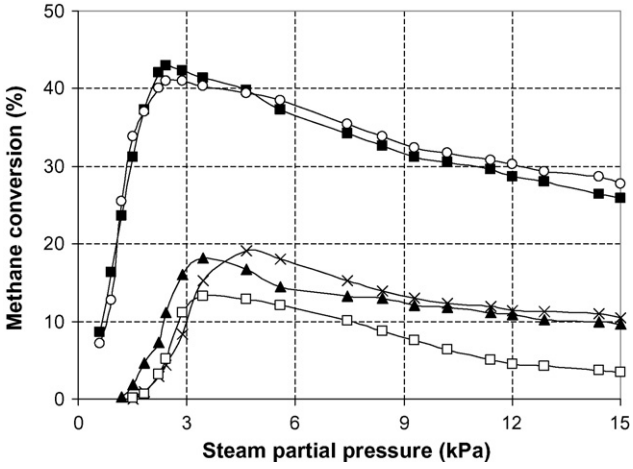

Fig. 8. Effect of steam partial pressure on steam reforming rate over different catalysts at 800 °C (Ni/Ce-ZrO_2 (HSA) (◯), Ni/CeO_2 (HSA) (■), Ni/Al_2O_3 (×), Ni/Ce-ZrO_2 (LSA) (▲), and Ni/CeO_2 (LSA) (□)).

Table 4
Dependence of inlet H_2O/CH_4 ratio on the amount of carbon formation on the catalyst surface (900 °C)

Catalysts	Amount of carbon formation at various H_2O/CH_4 ratios (mmol g_{cat}^{-1})							
	0	0.2	0.4	0.6	0.8	1.0	2.0	3.0
Ni/CeO_2 (HSA)	0.90	0.73	0.59	0.26	0.14	0.09	~0	~0
$Ni/Ce\text{-}ZrO_2$ (HSA)	1.04	0.85	0.54	0.21	0.07	~0	~0	~0
Ni/CeO_2 (LSA)	1.26	1.24	1.09	0.73	0.50	0.34	0.23	0.14
$Ni/Ce\text{-}ZrO_2$ (LSA)	1.30	1.18	0.79	0.56	0.32	0.18	0.09	~0
Ni/Al_2O_3	2.37	2.37	2.25	2.16	2.06	1.99	1.49	1.35

Table 5
Reaction orders in hydrogen from the methane steam reforming reaction at low hydrogen partial pressure (4 kPa CH_4, 12 kPa H_2O, and up to 5 kPa H_2)

Catalysts	Reaction order in hydrogen at different temperatures				
	650 °C	700 °C	750 °C	800 °C	850 °C
Ni/CeO_2 (HSA)	0.16	0.18	0.16	0.16	0.17
$Ni/Ce\text{-}ZrO_2$ (HSA)	0.17	0.18	0.19	0.16	0.17
Ni/CeO_2 (LSA)	0.17	0.18	0.19	0.18	0.17
$Ni/Ce\text{-}ZrO_2$ (LSA)	0.18	0.19	0.18	0.20	0.18
Ni/Al_2O_3	0.34	0.31	0.28	0.30	0.29

(HSA) and $Ni/Ce\text{-}ZrO_2$ (HSA) to achieve the maximum reforming reactivity were lower than the others.

The methane steam reforming in the presence of CO_2 was then investigated by adding different inlet CO_2 partial pressures (1–5 kPa) to the feed gas. Fig. 9 presents the effect of CO_2 on the reforming rate for each catalyst by plotting the relationship between $\ln(\text{Rate}_{\text{with } CO_2}/\text{Rate}_{\text{without } CO_2})$ and $\ln(P_{CO_2})$. As seen from this figure, CO_2 presented a negative effect on the CH_4 conversion for all catalysts; however, in contrast to the influence of H_2, the weaker inhibition effect by CO_2 was observed for Ni on ceria-based supports. According to the reaction order in CO_2 calculation, the reaction order in CO_2 for Ni/Al_2O_3 was approximately −0.12, whereas those over Ni on ceria-based supports were around −0.06 to −0.03, which clearly indicated the weaker inhibitory effect of CO_2 for Ni on ceria-based supports.

Finally, the methane steam reforming in the presence of O_2 (as autothermal reforming) was then carried out by adding different O_2 partial pressures (1–4 kPa) into the feed gas at several operating temperatures. The rate increased with increasing the inlet oxygen partial pressure for all catalysts as shown in Fig. 10. However, H_2 and $CO/(CO+CO_2)$ production selectivity were found to decrease with increasing O_2 concentration as shown in Fig. 11 for Ni/Al_2O_3, $Ni/Ce\text{-}ZrO_2$ (LSA), and Ni/CeO_2 (LSA) and Fig. 12 for $Ni/Ce\text{-}ZrO_2$ (HSA) and Ni/CeO_2 (HSA), respectively. It should be noted that, at the same operating conditions, the $CO/(CO+CO_2)$ production selectivity for Ni/Al_2O_3 was observed to be higher than that over Ni on ceria-based supports. The difference in this production selectivity is due to the reactivity toward the water-gas shift reaction of each support. The water-gas shift reaction (WGS) activities of each support was also carried out in the present work to ensure the influence of this reaction on the $CO/(CO+CO_2)$ selectivity. Fig. 13 shows the activities of all supports toward this reaction at several tem-

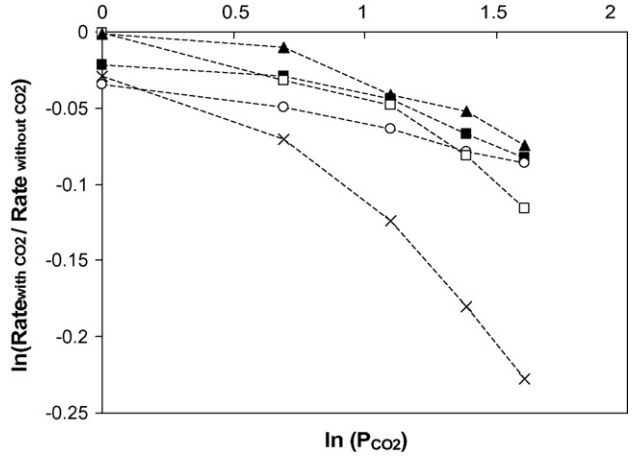

Fig. 9. Effect of carbon dioxide partial pressure on steam reforming rate over different catalysts at 800 °C ($Ni/Ce\text{-}ZrO_2$ (HSA) (◯), Ni/CeO_2 (HSA) (■), Ni/Al_2O_3 (×), $Ni/Ce\text{-}ZrO_2$ (LSA) (▲), and Ni/CeO_2 (LSA) (□)).

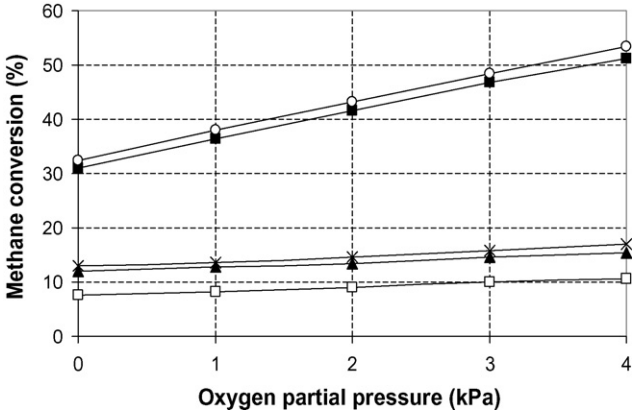

Fig. 10. Effect of oxygen partial pressure on steam reforming rate over different catalysts at 800 °C ($Ni/Ce\text{-}ZrO_2$ (HSA) (◯), Ni/CeO_2 (HSA) (■), Ni/Al_2O_3 (×), $Ni/Ce\text{-}ZrO_2$ (LSA) (▲), and Ni/CeO_2 (LSA) (□)).

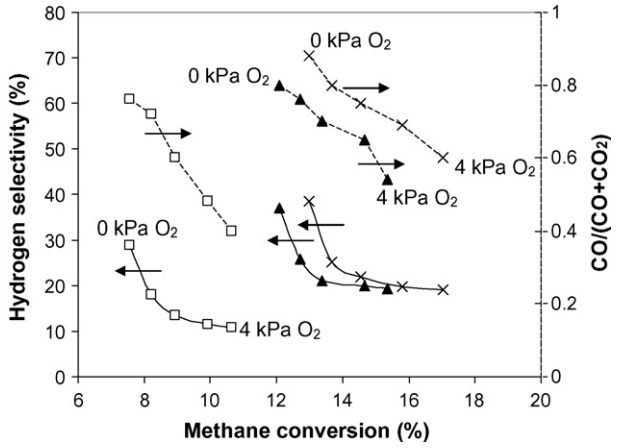

Fig. 11. Effect of oxygen partial pressure on the H_2 selectivity (solid lines) and $CO/(CO+CO_2)$ (dot lines) at isoconversion from steam reforming over Ni/Al_2O_3 (×), $Ni/Ce\text{-}ZrO_2$ (LSA) (▲), and Ni/CeO_2 (LSA) (□) at 800 °C.

peratures. Among the supports, the activity toward this reaction over CeO_2 (HSA) was the highest.

4. Discussion

Improvements of stability and activity toward methane steam reforming were achieved for Ni on high surface area (HSA) ceria-based supports. The high stability is due to the lower sintering rate compared to Ni on low surface area (HSA) ceria-based supports and the higher resistance toward carbon deposition compared to Ni/Al_2O_3, while the high reforming activity is possibly due to the improvement of Ni-dispersion on the high surface area support (Table 2), and also the strong gas–solid redox reaction between methane and the high surface area (HSA) ceria-based supports. It has been reported that the solid–gas reaction between CeO_2 and CH_4 produces synthesis gas with a H_2/CO ratio of two (Eq. (4)), while the reduced ceria can react with CO_2 and H_2O to recover CeO_2 and also produce CO and H_2 (Eqs. (5) and (6)) [39–41]. Importantly, we reported in our previous work that these redox reactions (Eqs. (4)–(6))

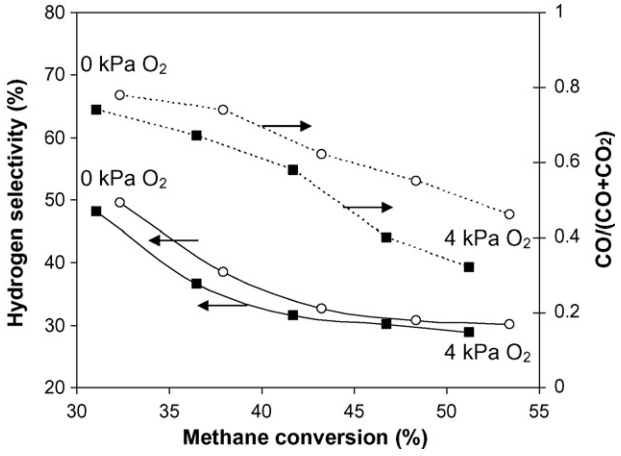

Fig. 12. Effect of oxygen partial pressure on the H_2 selectivity (solid lines) and $CO/(CO+CO_2)$ (dot lines) at isoconversion from steam reforming over $Ni/Ce\text{-}ZrO_2$ (HSA) (◯), and Ni/CeO_2 (HSA) (■) at 800 °C.

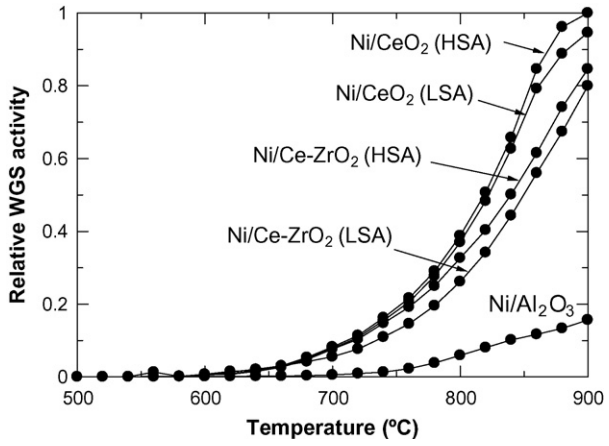

Fig. 13. The activities of each catalyst toward the water-gas shift reaction.

increase with increasing the specific active surface area of CeO_2 [42].

$$V_{O}^{\bullet\bullet} + 2e' + CO_2 = O_x + CO \quad (5)$$

$$V_{O}^{\bullet\bullet} + 2e' + H_2O = O_x + H_2 \quad (6)$$

The addition of suitable ratio of ZrO_2 over ceria, as $Ce\text{-}ZrO_2$, has also been widely reported to improve the oxygen storage capacity, and the redox reactivity of material [22–31]. These benefits were associated with enhanced reducibility of cerium (IV) in $Ce\text{-}ZrO_2$, which is a consequence of high O^{2-} mobility inside the fluorite lattice. The reason for the increasing mobility might be related to the lattice strain, which is generated by the introduction of a smaller isovalent Zr cation into the CeO_2 lattice (Zr^{4+} has a crystal ionic radius of 0.84 Å, which is smaller than 0.97 Å for Ce^{4+} in the same co-ordination environment).

The high resistance toward carbon deposition, which was observed from the catalyst over high surface area ceria-based supports, is also related to the facile redox reaction. During the steam reforming of methane, the following reactions are theoretically the most probable reactions that could lead to surface carbon formation:

$$2CO = CO_2 + C \quad (7)$$

$$CH_4 = 2H_2 + C \quad (8)$$

$$CO + H_2 = H_2O + C \quad (9)$$

$$CO_2 + 2H_2 = 2H_2O + C \quad (10)$$

Reactions (9)–(10) are favorable at low-temperatures, whereas the Boudouard reaction (Eq. (7)) and the decomposition of methane (Eq. (8)) are the major pathways for carbon formation at high-temperatures as they show the largest change in Gibbs energy. According to the range of temperature in this study, carbon formation would be formed via the decomposition of methane and Boudouard reactions. By applying ceria-based supports, the formation of carbon species via both reactions could be inhibited by the redox reactions with the lattice oxygen (O_x) forming H_2 and CO_2, which is thermodynamically unfavored to form carbon species in this range of conditions.

Therefore, significant lower amount of carbon deposition were consequently observed even at low inlet H_2O/CH_4 ratio.

The experiments on the effect of co-reactants yielded non-linear positive hydrogen trend. The positive effect at the low hydrogen appearance could be due to the reduction of oxidized state on the surface active site of nickel, while the inhibitory effect at high hydrogen partial pressure is due to the reverse methane steam reforming methanation, and the reverse water-gas shift reactions [1–3]. In addition, the presence of hydrogen atom on some active sites of nickel particle could also lead to the decrease in methane conversion [1–3]. Regarding the observed reaction order in hydrogen, the inhibitory impact for Ni catalysts on ceria-based supports (both HSA and LSA) is stronger than that for Ni/Al_2O_3 due to the redox property of the ceria-based materials. As described earlier, the gas-solid reaction between the ceria-based materials and CH_4 can generate CO and H_2, while the reduced state can react with steam and CO_2 to produce H_2 and CO, respectively. For $Ni/Ce\text{-}ZrO_2$ and Ni/CeO_2, although hydrogen prevents the oxidized state of nickel, this component can also reduce ceria via the reverse of Eq. (6) and consequently results in the inhibition of methane conversion via Eq. (4). This explanation is in good agreement with the previous studies [43] which investigated kinetics parameters for the methane steam reforming on ceria-based materials and reported the negative effect of hydrogen on methane conversion over these materials due to the change of Ce^{4+} to Ce^{3+}.

The dependence of H_2O on the CH_4 conversion is non-monotonic due to adsorption competition between CH_4 and H_2O on the catalyst active sites. Previous works [4,5] also reported the same results and explanation. The CH_4 conversion increased with increasing the inlet O_2 partial pressure. However, the $CO/(CO + CO_2)$ production selectivity and H_2 production rates strongly decreased with increasing O_2 partial pressure. This could be due to the combustion of H_2 and CO productions and the inhibition of H_2O adsorption on the catalyst surface active sites by O_2.

5. Conclusion

High surface area CeO_2 and $Ce\text{-}ZrO_2$ with Ce/Zr ratio of 3/1 are the good candidates to be used as the support for Ni catalysts for the steam reforming of CH_4 producing H_2 for later utilization in SOFC. The great advantages of Ni on high surface area (HSA) ceria-based supports are the high reforming reactivity, and also the high stability due to their excellent resistance toward carbon formation. Lower inlet H_2O/CH_4 ratio is required for Ni on high surface area (HSA) CeO_2 and $Ce\text{-}ZrO_2$ to prevent the carbon formation.

According to the effect of co-reactants (i.e. H_2O, H_2, CO_2, and O_2), the effects of H_2O on the methane steam reforming over Ni/CeO_2 (HSA) and $Ni/Ce\text{-}ZrO_2$ (HSA) are similar to those for Ni/Al_2O_3 in terms of reaction orders, whereas a stronger negative effect of H_2 was observed over Ni/CeO_2 (HSA) and $Ni/Ce\text{-}ZrO_2$ (HSA) as H_2 inhibits the gas-solid reaction between CeO_2 and CH_4. Additional of CO_2 inhibited the reforming rate, whereas addition of O_2 promoted the CH_4 conversion but reduced both CO and H_2 productions due to the further combustion and/or the inhibition of H_2O adsorption on the catalyst surface active sites. Lastly, the difference between Ni/CeO_2 (HSA) and $Ni/Ce\text{-}ZrO_2$ (HSA) is the $CO/(CO + CO_2)$ production selectivity. This selectivity for $Ni/Ce\text{-}ZrO_2$ is higher than that for Ni/CeO_2 due to the high reactivity toward water-gas shift reaction of CeO_2 compared to $Ce\text{-}ZrO_2$.

Acknowledgement

The financial support from The Thailand Research Fund (TRF) throughout this project is gratefully acknowledged.

References

[1] J. Xu, Ph.D. Thesis, Laboratorium Voor Petrochemische Techniek, Rijkuniversiteit, Gent, Belgium, 1986.
[2] J. Xu, G.F. Froment, AIChE 35 (1989) 88.
[3] J. Xu, G.F. Froment, AIChE 35 (1989) 97.
[4] S.S.E.H. Elnashaie, A.M. Adris, A.S. Al-Ubaid, M.A. Soliman, Chem. Eng. Sci. 45 (1990) 491.
[5] S.S.E.H. Elnashaie, S.S. Elshishini, Modeling, Simulation and Optimization of Industrial Fixed Bed Catalytic Reactors, Gordon and Breach Science Publishers, UK, 1993.
[6] X. Wang, R.J. Gorte, Appl. Catal. A 224 (2002) 209–218.
[7] H.S. Roh, K.W. Jun, W.S. Dong, J.S. Chang, S.E. Park, Y.I. Joe, J. Mol. Catal. A 181 (2002) 137–142.
[8] Q. Miao, G. Xiong, S. Sheng, W. Cui, L. Xu, L.X. Guo, Appl. Catal. A 154 (1987) 17–27.
[9] A.A. Lemonidou, M.A. Goula, I.A. Vasalos, Catal. Today 46 (1987) 175–183.
[10] W.S. Dong, H.S. Roh, K.W. Jun, S.E. Park, Y.S. Oh, Appl. Catal. A 226 (2002) 63–72.
[11] M. Mamak, N. Coombs, G. Ozin, Adv. Mater. 12 (2000) 198–202.
[12] M. Mamak, N. Coombs, G. Ozin, J. Am. Chem. Soc. 122 (2000) 8932.
[13] M. Mamak, N. Coombs, G.A. Ozin, Chem. Mater. 13 (2001) 3564.
[14] P. Bera, S. Mitra, S. Sampath, M.S. Hegde, Chem. Commun. (2001) 927.
[15] A. Martinez-Arias, J.M. Coronado, R. Cataluna, J.C. Conesa, J.C. Soria, J. Phys. Chem. B 102 (1998) 4357.
[16] D. Skarmoutsos, F. Tietz, P. Nikolopoulos, Fuel Cells 1 (2001) 243.
[17] T. Takeguchi, S.N. Furukawa, M. Inoue, J. Catal. 202 (2001) 14.
[18] J. Sfeir, P.A. Philippe, P. Moseki, N. Xanthopoulos, R. Vasquez, J.M. Hans, V.H. Jan, K.R. Thampi, J. Catal. 202 (2001) 229.
[19] N. Kiratzis, P. Holtappels, C.E. Hatchwell, M. Mogensen, J.T.S. Irvine, Fuel Cells 1 (2001) 211.
[20] H.S. Roh, W.S. Dong, K.W. Jun, S.E. Park, Chem. Lett. 88 (2001).
[21] P. Aguiar, E. Ramírez-Cabrera, N. Laosiripojana, A. Atkinson, L.S. Kershenbaum, D. Chadwick, Stud. Surf. Sci. Catal. 145 (2002) 387–390.
[22] M. Ozawa, M. Kimura, A. Isogai, J. Alloys Comp. 193 (1993) 73.
[23] G. Balducci, J. Kaspar, P. Fornasiero, M. Graziani, M.S. Islam, J. Phys. Chem. B 102 (1998) 557.
[24] G. Vlaic, P. Fornasiero, S. Geremia, J. Kaspar, M. Graziani, J. Catal. 168 (1997) 386.
[25] G.R. Rao, J. Kaspar, S. Meriani, R. Dimonte, M. Graziani, Catal. Lett. 24 (1994) 107.
[26] P. Fornasiero, R. Dimonte, G.R. Rao, J. Kaspar, S. Meriani, A. Trovarelli, M. Graziani, J. Catal. 151 (1995) 168.
[27] M. Haneda, K. Miki, N. Kakuta, A. Ueno, S. Tani, S. Matsura, M. Sato, Nihon Kagaku Kaishi (1990) 820.
[28] T. Ohata, Rare Earths 17 (1990) 37.
[29] J.G. Nunan, W.B. Williamson, H.J. Robota, SAE Paper 960768 (1996).
[30] S. Otsuka-Yao, H. Morikawa, N. Izu, K. Okuda, J. Jpn. Inst. Metals 59 (1995) 1237.
[31] M.H. Yao, T.E. Hoost, R.J. Baird, F.W. Kunz, J. Catal. 166 (1997) 67.
[32] C.T. Kresge, M.E. Leonowicz, W.J. Roth, J.C. Vartuli, J.S. Beck, Nature 359 (1992) 710.

[33] Q. Huo, D.I. Margolese, U. Ciesla, P. Feng, T.E. Gier, P. Sieger, R. Leon, P.M. Petroff, B. Schüth, G.D. Stucky, Nature 368 (1994) 317.
[34] P.T. Tanev, T.J. Pinnavaia, Science 267 (1995) 865.
[35] U. Ciesla, S. Schacht, G.D. Stucky, K.K. Unger, F. Schüth, Angew. Chem. Int. Ed. Engl. 35 (1996) 541.
[36] D.M. Antonelli, J.Y. Ying, Angew. Chem. Int. Ed. Engl. 35 (1996) 426.
[37] Q. Huo, D.I. Margolese, U. Ciesla, D.G. Demuth, P. Feng, T.E. Gier, P. Sieger, A. Firouzi, B.F. Chmelka, B. Schüth, G.D. Stucky, Chem. Mater. 6 (1994) 1176.
[38] Daniela Terribile, Alessandro Trovarelli, Jordi Llorca, Carla de Leitenburg and Giuliano Dolcetti, Catal. Today 43 (1998) 79–88.
[39] K. Otsuka, T. Ushiyama, I. Yamanaka, Chem. Lett. (1993) 1517.
[40] K. Otsuka, M. Hatano, A. Morikawa, J. Catal. 79 (1983) 493.
[41] K. Otsuka, M. Hatano, A. Morikawa, Inorg. Chim. Acta 109 (1985) 193.
[42] N. Laosiripojana, S. Assabumrungrat, Appl. Catal. B: Environ. 60 (2005) 107.
[43] E. Ramirez, A. Atkinson, D. Chadwick, Appl. Catal. B 36 (2002) 193–206.